Title Page

Title: COMT-catalyzed palmitic acid methyl ester biosynthesis in perivascular adipose tissue and its potential role against hypertension

Authors: Chin-Hung Liu,[1,4,5] Hao-Jen Hsu,[3] Tzu-Ling Tseng,[2,5] Tsung-Jen Lin,[1,4] Wei-Hsiang Weng[3], Mei-Fang Chen[2,5*] and Tony Jer-Fu Lee[2,5,6*]

(*) equal contribution

Affiliations:

[1]Department of Pharmacology, College of Medicine, Tzu Chi University, Hualien, Taiwan

[2]Department of Medical Research, Hualien Tzu Chi Hospital, Buddhist Tzu Chi Medical Foundation, Hualien, Taiwan

[3]Department of Life Sciences, College of Medicine, Tzu Chi University, Hualien, Taiwan

[4]Ph.D program in Pharmacology and Toxicology, Department of Medicine, School of Medicine, Tzu Chi University, Hualien, Taiwan

[5]Cardiovascular Research Center, Hualien Tzu Chi Hospital, Buddhist Tzu Chi Medical Foundation, Hualien, Taiwan

[6]Department of Pharmacology, Southern Illinois University School of Medicine, Springfield, USA

Running title: COMT-mediated PAME biosynthesis

Corresponding author: Mei-Fang Chen, Department of Medical Research, Hualien Tzu Chi Hospital, 707, Sec 3, Chung Yang Road Hualien, Taiwan 970; Phone: +886-3-8561825 #16613; FAX: +886-3-8573710; E-mail: mfchen@mail.tcu.edu.tw

Number of words in the abstract: 250

Number of words in Introduction: 457

Number of words in Discussion: 908

Number of text pages: 25

Number of tables: 2

Number of figures: 7

Number of supplementary figures: 6

Number of references: 57

Non-standard abbreviations:

3'-hydroxy-4'-methoxyacetophenone, 3H4MAP; 4H3MAP, 4'-hydroxy-3'-methoxyaceto-phenone; AdoMet, *S*-5'-adenosyl-*L*-methionine; Adox, adenosine-2',3'-dialdehyde; AT1, Ang II receptor type 1; Catechol-O-methyltransferase, COMT; DHAP, 3,4-dihydroxyaceto-phenone; DNC, 3,5-dinitrocatechol; FAME, fatty acid methyl ester; GC-MS, gas chromatography-mass spectrometry; MD, molecular dynamics; MM/PBSA, Molecular Mechanics Poisson-Boltzmann Surface Area; MOE, Molecular Operating Environment; PA, palmitic acid; PAME, palmitic acid methyl ester; PVAT, perivascular adipose tissue; PVATRF, PVAT-derived relaxing factor; SHR, spontaneously hypertensive rat; WKY, Wistar Kyoto.

Recommended section assignment: Cardiovascular

Abstract

Decreased release of palmitic acid methyl ester (PAME), a vasodilator, from perivascular adipose tissue (PVAT) might contribute to hypertension pathogenesis. However, the PAME biosynthetic pathway remains unclear. In this study, we hypothesized that PAME is biosynthesized from palmitic acid (PA) via human catechol-O-methyltransferase (COMT) catalysis and that decreased PAME biosynthesis plays a role in hypertension pathogenesis. We compared PAME biosynthesis between age-matched normotensive Wistar Kyoto (WKY) rats and hypertensive spontaneously hypertensive rats (SHRs) and investigated the effects of losartan treatment on PAME biosynthesis. Computational molecular modeling indicated that PA binds well at the active site of COMT. Furthermore, in *in vitro* enzymatic assays in the presence of COMT and *S*-5'-adenosyl-*L*-methionine (AdoMet), the stable isotope [$^{13}C_{16}$]-PA was methylated to form [$^{13}C_{16}$]-PAME in incubation medium or the Krebs–Henseleit solution containing 3T3-L1 adipocytes or rat PVAT. The adipocytes and PVATs expressed membrane-bound (MB)-COMT and soluble (S)-COMT proteins. [$^{13}C_{16}$]-PA methylation to form [$^{13}C_{16}$]-PAME in 3T3-L1 adipocytes and rat PVAT was blocked by various COMT inhibitors, such as *S*-(5'-adenosyl)-*L*-homocysteine, adenosine-2',3'-dialdehyde, and tolcapone. MB- and S-COMT levels in PVATs of established SHRs were significantly lower than those in PVATs of age-matched normotensive WKY rats, with decreased [$^{13}C_{16}$]-PA methylation to form [$^{13}C_{16}$]-PAME. This decrease was reversed by losartan, an Ang II type 1

receptor antagonist. Therefore, PAME biosynthesis in rat PVAT is dependent on AdoMet, catalyzed by COMT, and decreased in SHRs, further supporting the role of PVAT/PAME in hypertension pathogenesis. Moreover, the antihypertensive effect of losartan might be due partly to its increased PAME biosynthesis.

Significance Statement:

PAME is a key PVAT-derived relaxing factor. We for the first time demonstrate that PAME is synthesized through PA methylation via the AdoMet-dependent COMT catalyzation pathway. Moreover, we confirmed PVAT dysfunction in the hypertensive state. COMT-dependent PAME biosynthesis is involved in AT-1 receptor-mediated blood pressure regulation, as evidenced by the reversal of decreased PAME biosynthesis in PVAT by losartan in hypertensive rats. This finding might help in developing novel therapeutic or preventive strategies against hypertension.

Introduction

The significant roles of PVAT in regulating the vascular tone (Lee et al., 2011; Eringa et al., 2012) and vascular homeostasis (Chang et al., 2012; Szasz et al., 2013) are well recognized. PVATs of different vascular beds release both dilative and constrictive factors according to the body's need. Among these factors, PVAT-derived relaxing factors (PVATRFs) have attracted much interest (Tano et al., 2014). Several substances, such as adiponectin (Fesus et al., 2007; Xu et al., 2010), hydrogen sulfide (Wojcicka et al., 2011), nitric oxide (Gao et al., 2007), and prostaglandin I_2, are considered as a PVATRF. PAME, a novel vasodilator that attenuates the constrictor-mediated active response is released from PVAT and is also considered as a PVATRF (Lee et al., 2011).

In SHR animals, PAME amount released from PVAT and PVAT-related relaxation decrease in aorta, which can be reversed by losartan, an antihypertensive drug (Lee et al., 2011). PAME levels in PVAT might play a role in hypertension pathogenesis. In addition, PAME might enhance cerebral blood flow, alleviate neuronal cell death, and improve cognitive functions in animals subjected to asphyxial cardiac arrest (Lee et al., 2018). Although the evidences for physiological roles of PAME are emerging, the PAME biosynthesis in PVAT remains unknown.

COMT (EC 2.1.1.6) is an AdoMet-dependent enzyme (Mannisto and Kaakkola, 1999). The main function of COMT is to degrade various catecholamines (e.g., dopamine, epinephrine, and norepinephine) (Hirano et al., 2007) and catecholestrogens (e.g., 2-hydroxyestradiol)

(Hernandez et al., 2013) via *O*-methylation. The binding for AdoMet, Mg^{2+}, and catechol-substrate are strictly controlled in a catalytic circle (Ma et al., 2014). After AdoMet, Mg^{2+} and substrate bind to COMT, the methyl group attached to the methionine sulfur atom of AdoMet is oriented toward the substrate-binding site for methylation (Ma et al., 2014). Most tissues, including adipose, contain two forms of COMT, membrane-bound (MB) and soluble (S) forms (Borchardt and Huber, 1975; Song et al., 2019).

Changes in COMT activity or expression have been implicated in hypertension and heart failure (Houston, 2007). The systolic blood pressure is significantly increased in *COMT*$^{-/-}$ mice (Kanasaki et al., 2008; Stanley et al., 2012). The human genotypic variant of functional COMT Val158Met is related to hypertension risk (Stewart et al., 2009; Htun et al., 2011). Previous studies have demonstrated decreased MB-form COMT activity and protein expression in the liver (Tsunoda et al., 2003), brain (Masuda et al., 2006), and renal cortex (Ooshima et al., 2009) of SHRs compared with those of age-matched normotensive WKY rats.

In this study, we hypothesized that PAME is biosynthesis from PA via COMT catalysis, and that the decreased PAME biosynthesis is involved in hypertension pathogenesis. We compared PAME biosynthesis between age-matched normotensive WKY rats and hypertensive SHRs, and investigated the effect of losartan treatment on PAME biosynthesis.

Materials and methods

Animals and aortic PVAT sampling

Adult male Sprague-Dawley (SD) rats (body weight, 350–400 g), 8- and 13-week-old male SHRs, 8- and 13-week-old male WKY rats (BioLASCO Co., Ltd. Taipei, Taiwan) were housed in the animal quarters at Tzu Chi University, Taiwan, under a 12/12 h light/dark cycle. All rats were fed a standard ration and provide tap water *ad libitum*. The rats were anesthetized using penotobarbital, and PVAT surrounding the thoracic aorta was quickly excised and processed for PAME biosynthesis, COMT protein expression, and immunocytochemistry studies.

This study was performed in accordance with the ethical principles of animal research, and the animal protocol was approved by the ethics committee of Tzu Chi University.

Measurement of the arterial blood pressure

Systolic blood pressure was measured by the tail-cuff method using a programmed MK-2000ST electro sphygmomanometer (Muromachi, Tokyo, Japan), as described previously (Chou et al., 2013). Table 1 shows systolic blood pressure data.

Chemicals, substrates and reagents

AdoMet, *S*-(5'-adenosyl)-*L*-homocysteine (AdoHcy), adenosine-2',3'-dialdehyde (Adox), COMT, [$^{13}C_{16}$]-PA, tolcapone, 3,4-dihydroxyacetophenone (DHAP), 3'-hydroxy-4'-methoxyacetophenone (3H4MAP), 4'-hydroxy-3'-methoxyacetophenone

(4H3MAP), N-tris(hydroxymethyl)-methyl-2-aminoethane sulphonic acid (TES), methyl pentadecanoate, PAME and losartan were purchased from Sigma-Aldrich (St. Louis, MO, USA). Ethyl acetate, ethanol and hexane were purchased from Mallinckrodt (St. Louis, MO, USA).

Computational modeling analysis of human S-COMT

Molecular docking

First, three ligands DHAP (a standard ligand for COMT), 3,5-dinitrocatechol (DNC; a competitive COMT inhibitor), and PA selected for molecular docking were constructed using MOE2013.08 (Molecular Operating Environment, http://www.chemcomp.com). Ligand topologies for subsequent simulations were obtained from the GlycoBioChem PRODRG2 web server (http://davapc1.bioch.dundee.ac.uk/cgi-bin/prodrg), provided by Professor Daan van Aalten (Schuttelkopf and van Aalten, 2004) under the GROMOS 53A6 force field, which is also suitable for biomolecules. The receptor apo–human S-COMT (Protein Data Bank code: 3A7E) lacking DNC ligand (only COMT, AodMet, and Mg^{2+}) was set as a receptor for binding various ligands. The initial favorable sites for the binding of each ligand to apo–S-COMT were determined using the docking module of MOE2013.08.

Molecular dynamics simulations

The DNC-apo-S-COMT complex was placed in an 80 Å × 80 Å × 80 Å water box containing more than 10,000 water molecules. To neutralize DNC-apo-S-COMT binding, 48

Na^+ and 43 Cl^-, forming a 100 mM NaCl solution, were added following energy minimization. A total of 45,672 atoms of the complex consisted 2090 atoms of COMT, 36 atoms of AdoMet, 18 atoms of DNC, 1 Mg^{2+}, and 14,479 simple point-charge water molecules, including 48 Na^+ and 43 Cl^-. All molecular dynamics (MD) simulations were run for 200 nanoseconds (ns) to calculate the binding free energy (Table 2). Detailed MD simulation methods and equilibration protocols have been described previously (Liou et al., 2014).

MM/PBSA-binding free energy calculations

To define the most stable complexes predicted by molecular docking, the Molecular Mechanics Poisson-Boltzmann Surface Area (MM/PBSA) approach was used for estimating the binding free energy (ΔG_{bind}) on the basis of snapshots extracted from a single trajectory of the DNC-apo-S-COMT complex (single-trajectory method) (Hou et al., 2011b; Hou et al., 2011a). The single-trajectory method is much faster and requires less sampling than the individual trajectory method, which requires three separate MD simulations on system components (receptor, ligand, and complex) (Hou and Yu, 2007; Xu et al., 2013). We assumed that the receptor and ligand behaved similarly during binding, which was reasonable and adoptable for our simulations. The free energy calculations have been explained in detail previously (Jiang et al., 2015; Chang et al., 2017). To calculate all energy terms, extracted 300 snapshots from 30 (170-200)-ns molecular docking trajectories per system.

In vitro enzymatic assay of COMT-catalyzed biosynthesis from PA

We assayed COMT activity *in vitro* as described by Tehlivets (Tehlivets, 2011). Briefly, we placed glass tubes on ice. To evaluate the *O*-methylation of DHAP dissolved in deionized water (positive control) or [$^{13}C_{16}$]-PA dissolved in absolute ethanol, we incubated 100 μM of either substrate with COMT enzyme extracted from porcine liver (C1897, Sigma-Aldrich) of 10–30 units from a stock solution of 1000 units/mL of COMT in cold TES diluent buffer at pH 7.6 in the presence of 1.2 mM $MgCl_2$ and 4 mM dithiothreitol. The reaction was initiated by adding 1 mM AdoMet for 1 h at 37℃ and then terminated by adding 0.2 M sodium borate (pH 10.0). The reaction products were analyzed for methylated DHAP (3H4MAP and 4H3MAP) or [$^{13}C_{16}$]-PAME using a spectrophotometer and gas chromatography-mass spectrometry (GC-MS), respectively; absorbance was measured at 344 nm. Mediums containing no AdoMet (blank) or COMT enzyme served as negative controls. The assay was linear over a range of concentrations from 1-100 μM with a correlation coefficient of r^2 = 0.9998 ($p < 0.0001$) for *O*-methylated DHAP and 0.9972 ($p < 0.0001$) for PAME.

GC-MS

Reaction samples from *in vitro* enzymatic assays, condition mediums, and Krebs-Henseleit solution from incubation with 3T3-L1 adipocytes and isolated PVAT preparations were added with 10 μM pentadecanoic acid methyl ester, which acts as internal standard. Next, the samples were lyophilized and resolved using ethyl acetate to further dissolve the organic compounds, as described previously (Lin et al., 2008; Lee et al., 2011). After vortexing,

sonicating, and centrifuging at 1500 rpm for 5 min at 4°C, the supernatant was transferred to a glass sample vial to form a 2-μL splitless injection. The samples were detected using a Hewlett-Packard Model 6890 GC system (Hewlett-Packard, Palo Alto, CA USA) assembled with a G1512A autosampler and interfaced to a 5973 mass selective detector. An HP-5MS 5% phenyl polysilphenylene-siloxane capillary column (10 m × I.D. 0.32 mm; film thickness 0.5 μm) was used; helium gas was used as the carrier gas at a flow rate of 0.7 mL/min. The temperatures of the GC injection port and interface were maintained at 250℃ and 300℃, respectively. The starting temperature of GC was set at 90℃, which was increased to 240℃ at 15℃/min and then increased up to 300℃ at 10℃/min. Mass spectrum scanning was set at 50–500 *m*/*z* and the electron ionization energy of the electron impact mode was set at 70 eV. Hewlett-Packard G1701AA version 0.300 ChemStation Software was used for data acquisition and analysis in the drug analysis mode. *O*-methylated PAME (M^+, 270 *m/z*) and [$^{13}C_{16}$]-PAME (M^+, 286 *m/z*) were analyzed with single diagnostic ion-based GC-MS (Supplementary Figure 1) to qualitatively and quantitatively analyze PAME and [$^{13}C_{16}$]-PAME, as described previously (Lin et al., 2008; Lee et al., 2010; Lee et al., 2011).

3T3-L1 adipocyte culture and differentiation

Mouse embryo pre-adipocyte (fibroblasts) 3T3-L1 cells were obtained from the American Type Culture Collection (ATCC®) and cultured in 12-well cluster plates in Dulbecco's Modified Eagle's Medium (DMEM; HyClone, Logan, UT, USA) supplemented with 10%

calf serum (Gibco, Grand Island, NY, USA) and 1% antibiotics (Invitrogen, Carlsbad, CA, USA) until confluence, as described previously (Lee et al., 2011). Two days after confluence (day 0), the fibroblasts were exposed to a differentiation medium comprising 0.5 mM isobutylmethylxanthine, 1 μM dexamethasone, 1.67 mM insulin (MDI; Sigma-Aldrich), and 10% fetal bovine serum for 3 days. Finally, the differentiated 3T3-L1 adipocytes were transferred to DMEM with 1.67 mM insulin and 10% fetal bovine serum and re-fed every 2 days. Mature 3T3-L1 adipocytes were confirmed using Oil Red O staining of lipid droplets in adipocytes.

Oil Red O staining

Lipid droplets in mature 3T3-L1 adipocytes were stained with Oil Red O, as described previously with some modifications (Kawai et al., 2007). Briefly, 3T3-L1 adipocytes were fixed with 4% formaldehyde-phosphate buffer (pH 7.4) for 1 h, rinsed with water, and stained with 0.3% filtered Oil Red O (Sigma-Aldrich) in 100% isopropanol for 1 h at 60℃. Then, the cells were washed twice with distilled water to remove excess dye and photographed under a Leica light microscope (Leica Microsystems, Wetzlar, Germany).

PAME biosynthesis in 3T3-L1/PVAT adipocytes and effects of COMT inhibitors

3T3-L1 adipocytes were incubated in 12-well cluster with different concentrations of [$^{13}C_{16}$]-PA (100–500 μM) dissolved in absolute ethanol in 1 mL culture medium (24 and 72 h) in a 5% CO_2 incubator at 37℃. Culture medium containing 500 μM [$^{13}C_{16}$]-PA without

3T3-L1 adipocytes was used as a control. AdoHcy, a COMT-catalyzed AdoMet metabolite, inhibits AdoMet-dependent methyltransferases via the feedback inhibitory mechanism (Yeh et al., 1991). Therefore, we determined whether AdoHcy inhibits PAME biosynthesis in 3T3-L1 adipocytes. Different concentrations (100 and 300 μM) of AdoHcy in dimethyl sulfoxide were added to incubation mediums containing 250 μM [$^{13}C_{16}$]-PA and 3T3-L1 adipocytes. Culture medium containing 250 μM [$^{13}C_{16}$]-PA without 3T3-L1 adipocytes was used as a negative control, and cells treated with an equivalent amount of [$^{13}C_{16}$]-PA and dimethyl sulfoxide (<0.1%; solvent for dissolving AdoHcy) were as a positive control. We used similar procedures to examine the effects of other COMT inhibitors on PAME biosynthesis, including 10 and 100 μM Adox (an inhibitor for AdoHcy hydrolase/EC 3.3.1.1) in dimethyl sulfoxide and 1–1000 nM tolcapone (a highly selective COMT inhibitor) in dimethyl sulfoxide (Vieira-Coelho and Soares-da-Silva, 1999). By inhibiting AdoHcy hydrolase, which catalyzes AdoHcy hydrolysis to form adenosine and homocysteine (Bartel and Borchardt, 1984), Adox acts as an indirect AdoMet-dependent MTase inhibitor by increasing AdoHcy concentration (Kurkela et al., 2004). Finally, all culture mediums were collected and processed for GC-MS analysis.

To determine PAME biosynthesis in rat thoracic aortic PVAT (350–400 g SD, 8- and 13-week-old SHRs or WKY rats), isolated PVAT was incubated in 10 mL Krebs-Henseleit solution with 250 μM [$^{13}C_{16}$]-PA dissolved in absolute ethanol for 1–90 min at 37℃.

Krebs-Henseleit solution with 250 μM [$^{13}C_{16}$]-PA without PVAT was used as a negative control. To determine whether COMT inhibitors (tolcapone) inhibit PAME biosynthesis in rat thoracic aortic PVAT, isolated PVAT was pre-incubated in 10 mL Krebs-Henseleit solution containing different concentrations of tolcapone (300 nM and 1 μM) for 30 min at 37℃. Pre-incubated PVAT was then transferred to a different tissue bath containing 10 mL Krebs-Henseleit solution and 250 μM [$^{13}C_{16}$]-PA dissolved in absolute EtOH and incubated for 1–90 min at 37℃. In addition, isolated PVAT preparations (from 13-week-old SHRs or WKY rats) were incubated in 10 mL Krebs-Henseleit solution containing 1 μM losartan in dimethyl sulfoxide alone or 1 μM losartan plus tolcapone in dimethyl sulfoxide for 30 min. Krebs-Henseleit solution containing 250 μM [$^{13}C_{16}$]-PA without PVAT was used as a negative control. All samples were collected and processed for GC-MS assay. Cumulative [$^{13}C_{16}$]-PAME concentrations from different incubation periods were calculated from the area under the curve.

Western blots

Bicinchoninic acid (BCA) assay (Pierce Chemicals, Rockford, IL, USA) was used for protein quantification. Cell/tissue extracts were diluted by adjunction of 4 parts of sample buffer (0.25 M Tris-HCl, pH 6.8; 2% 2-mecaptoethanol, 8% sodium dodecyl sulfate, 0.02% bromophenol blue and 40% glycerol) and boiled for 5 min at 100℃. Protein extracts were quantified. Then, 20 mg of each protein was separated on 10% SDS polyacrylamide gel and

transferred onto polyvinylidene difluoride membranes (Bio-Rad, Hercules, CA, USA) using semidry electroblotting (Amersham Biosciences, Buckinghamshire, UK). Polyvinylidene difluoride membranes were blocked with 5% non-fat milk/0.25% Tris-buffered saline containing Tween 20 for 2 h at room temperature. The mouse COMT monoclonal immunoglobulin G (IgG) antibody (1:2000; BD Transduction, CA, USA), anti-actin antibody (1:4000; Chemicon, IL, USA) or anti-tubulin antibody (1:4000; Chemicon, IL, USA) was incubated overnight at 4℃, and horseradish peroxidase-conjugated secondary antibodies (1:2000; KPL, Washington DC, USA) were added for 1 h at RT. Proteins expression was detected using a Biospectrum 810 UVP system (Thermo Fisher Scientific, Waltham, MA, USA) with enhanced chemiluminescence reagent (PerkinElmer Life Science, MA, USA). ImageJ v1.51 (National Institute of Mental Health, Bethesda, MD, USA) was used for proteins analysis (Tseng et al., 2012).

COMT immunofluorescence staining in rat aortic PVAT

Standard immunofluorescence staining techniques were used to demonstrate COMT immunoreactivities in 8- and 13-week-old SHR or WKY rat aortic PVAT (Tseng et al., 2016). Briefly, 2-μm-thick sections of paraffin-embedded PVAT were processed through antigen retrieval buffer and permeabilized with Triton X-100 for 30 min. Their non-specific interaction with antibodies was blocked by incubation with normal serum (BiogenX) for 1 h. After washed 3 times with buffer, the samples were allowed to interact with purified

anti-COMT mouse antibody (1:200; BD Bioscience, NJ, USA) overnight at 4℃ and anti-mouse IgG labeled with Hilyte Fluor 555 (1:200; AnaSpec) for 2 h. Cell nuclei were counter-stained with 4',6-diamidino-2-phenylindole (1:200; KPL) for 20 min. All sections were mounted with a water-soluble mounting media and examined under a Leica fluorescence microscope (Leica Microsystems). A few sections were processed by incubation with primary antibodies but without secondary antibodies serving as a negative control.

Hematoxylin-eosin Y staining

Rat aortas with the intact PVAT surrounding were sectioned and examined by using standard Hematoxylin-eosin Y staining technique as previously described (Tseng et al., 2012). Briefly, 2-μm paraffin-embedded cross-sections were placed on the slides. After deparaffinized with a non-xylene solution (Sigma-Aldrich), the specimens were rehydrated with a serial immersion in 100% for 3 min twice, 95% for 1 min, and 75% for 1 min of ethanol. Then, the samples were stained with hematoxylin for 3 min, and subsequently with eosin Y for 45 sec. After incubated in non-xylene solution for 6 min, the specimens were mounted with coverslips and examined under a light microscope (Olympus, Tokyo, Japan)(Figure 4 and Supplementary Figure 6).

Statistical analysis

Statistical analyses were performed using one-way analysis of variance and Student's *t*-test. *Post hoc* comparisons between groups were performed using Bonferroni's multiple

comparison test. Experimental data are presented as means and standard error of the mean (SEM). All data were analyzed using SPSS v. 18.0 (SPSS Inc., Chicago, IL, USA). $P < 0.05$ was considered as statistically significant.

Results

Molecular docking between PA and S-COMT using computational modeling

Computational molecular modeling analysis demonstrated that PA binds to S-COMT at a specific substrate pocket, which is appropriate for methylation in the presence of AdoMet and Mg^{2+} (Figure 1A). The predicted complex structure of DNC/S-COMT by computational molecular modeling was superposed with that of the crystal structure for comparison. The predicted binding position of DNC with S-COMT was at the binding pocket, which is quite similar to that of the crystal structure. By modeling, PA and DHAP bound to the same pocket of S-COMT as DNC did.

The root-mean-square deviations for PA, DNAP and DNC binding to S-COMT fluctuated from 0.1 to 0.28 nm. This result indicates that PA can stabilize at the binding pocket of S-COMT, similar to DNAP and DNC binding to S-COMT (Figure 1B).

Table 2 summarizes the free energy levels for PA, DNAP, and DNC binding to S-COMT. ΔG_{bind} for DNC binding (–61.49 ± 14.64 Kcal/mol) was lower than that for PA (–40.97 ± 20.37 Kcal/mol) and DHAP (122.77 ± 13.23 Kcal/mol) binding. ΔG_{bind} for PA–S-COMT was

between that for DHAP–S-COMT and DNC–S-COMT, indicating that the binding affinity of PA is stronger than that of DHAP but weaker than that for DNC.

COMT-catalyzed PAME biosynthesis from PA

To determine whether COMT plays a role in PA methylation during PAME biosynthesis, we administered a synthetic stable isotope [$^{13}C_{16}$]-PA to distinguish the sources of methylated products. *In vitro* enzymatic assays showed that [$^{13}C_{16}$]-PA was concentration-dependently transformed to [$^{13}C_{16}$]-PAME in the presence of COMT and AdoMet. As a positive control, DHAP formed 3H4MAP/4H3MAP after the addition of COMT and AdoMet. ~~but~~ However, no methylated products of DHAP or [$^{13}C_{16}$]-PA were detected in the absence of COMT or AdoMet (Figure 2A). The 100 or 500 μM [$^{13}C_{16}$]-PA were added to culture plates containing pre-adipocytes (undifferentiated fibroblasts) or 3T3-L1 adipocytes (differentiated). [$^{13}C_{16}$]-PAME concentrations in the medium with 3T3-L1 adipocytes were significantly higher than those in the medium with pre-adipocytes (Figure 2B and Supplementary Figure 2). In addition, both MB-COMT and S-COMT were expressed in pre-adipocytes and 3T3-L1 adipocytes, with higher expression for the latter than for the former (Figure 2 C, D and Supplementary Figure 4).

Blockade of PAME biosynthesis by COMT inhibitors in 3T3-L1 and PVAT adipocytes

Substrate inhibitors as shown in the scheme (Figure 1C), AdoHcy (100 and 300 μM) and Adox (10 and 100 μM), suppressed endogenous PAME and [$^{13}C_{16}$]-PAME biosynthesis in

differentiated 3T3-L1 adipocytes (Figure 3A). Tolcapone, a highly selective COMT inhibitor (1–1000 nM), also inhibited endogenous PAME and [$^{13}C_{16}$]-PAME accumulation in the culture medium of differentiated 3T3-L1 adipocytes (Figure 3B). *In vivo*, PVAT is located neighboring the arterial wall and mainly composed of adipocytes as shown in Figure 4. PAME released from PVAT is an important factor to regulate the vascular tension. [$^{13}C_{16}$]-PAME synthesis in Krebs-Henseleit solution following incubation with PVAT isolated from SD rats (Supplementary Figure 3), WKY rats and SHRs (Figure 5A, B) was also detected in the presence of 250 μM [$^{13}C_{16}$]-PA. Increase in [$^{13}C_{16}$]-PAME concentration was time-dependent. The peak concentration was reached after 30 min of incubation and gradually decreased after 45 min of incubation. PVAT pre-incubation with 300 nM or 1 μM tolcapone for 30 min decreased [$^{13}C_{16}$]-PAME generation, regardless of whether PVAT was isolated from SD rats, WKY rats or SHRs.

Losartan reverses the decreased PAME biosynthesis in established SHR PVAT

More [$^{13}C_{16}$]-PAME was synthesized in 13-week-old WKY rats than in 8-week-old WKY rats. Conversely, less [$^{13}C_{16}$]-PAME was synthesis from [$^{13}C_{16}$]-PA in PVAT of 13-week-old SHRs than that of 13-week-old WKY rats (Figure 5B). In 13-week-old established SHRs, the suppressed [$^{13}C_{16}$]-PAME biosynthesis was recovered to normal following the pre-incubation of PVAT with 1 μM losartan (n = 5). However, [$^{13}C_{16}$]-PAME biosynthesis remained unaffected in 13-week-old normotensive WKY rats (n = 5). Pre-incubation with 1 μM

JPET Fast Forward. Published on February 18, 2020 as DOI: 10.1124/jpet.119.263517
This article has not been copyedited and formatted. The final version may differ from this version.

tolcapone decreased [$^{13}C_{16}$]-PAME biosynthesis in both 13-week-old SHRs and WKY rats (*n* = 5).

COMT expression in PVAT of SHRs and WKY rats

Similar to 3T3-L1 adipocytes, the PVAT of 8- and 13-week-old SHRs and WKY rats showed MB-COMT and S-COMT expression (Figure 5C, D and Supplementary Figure 5). The 8-week-old pre-hypertensive SHRs, which showed normal systolic blood pressure compared with age-matched WKY rats (Table 1), showed almost similar MB- and S-COMT expression in aortic PVAT to age-matched WKY rats. In contrast, 13-week-old SHRs, which exhibited significantly higher systolic blood pressure than age-matched WKY rats (Table 1), and expressed showed lower MB- and S-COMT expression in aortic PVAT than age-matched controls (Figure 5C, D and Supplementary Figure 5).

COMT-expressing adipocytes in PVAT

The existence of COMT enzyme in PVAT were demonstrated by the presence of COMT-immunoreactive adipocytes (Figure 6; *n* = 12). COMT-immunofluorescence was localized in the cytoplasmic compartment except lipid droplet in adipocytes. However, no COMT-immunofluorescence was detected when primary or secondary antibodies were excluded during incubation (negative control).

Discussion

PAME is a PVATRF that drastically decreases in established SHRs (Lee et al., 2011). However, how PAME is synthesized in PVAT remains unclear. *In test tube*, PAME is synthesized from PA and AdoMet by COMT, a *O*-methylation enzyme (as depicted in Figure 1C). In cell level, PAME is also generated in 3T3L1 and PVAT adipocytes, which contain COMT enzyme. A schematic diagram (Figure 7) illustrates PAME biosynthesis in PVAT adipocytes. PAME biosynthesis is inhibited by different COMT inhibitors. In the hypertensive rat model, COMT expression as well as PAME generation in isolated PVAT was lower in established SHRs than in age-matched WKY rats.

Computational molecular modeling analysis revealed stable binding of PA to the binding pocket of S-COMT formed by AdoMet and Mg^{2+}, as evidenced by root-mean-square deviation simulations in which the PA–S-COMT complex was continuously stabilized at the distances (O–C) of 0–200 ns. Interestingly, although PA does not contain a catechol structure, PAME was synthesized by PA methylation via COMT catalysis as simulated in computational molecular modeling, and as demonstrated in *in vitro* enzymatic assays and pharmacological inhibitor experiments. Typically, PA is one of the most common saturated fatty acids found in the human body and can be obtained through diet and endogenous synthesis via *de novo* lipogenesis or lipolysis from triacylglycerol (TG) in adipose tissue. However, excess endogenous PA might induce endoplasmic reticulum stress (Tse et al., 2018) and lipotoxicity

in various cell types (Peng et al., 2011). It has been believed that degradation, desaturation and elongation of PA might be protective, and regulated by homeostasis mechanisms to prevent cells from lipid-related stress-induced damage (Green and Olson, 2011). In addition, methylation might be an alternative means to reduce PA-induced stress in the human body.

Endogenous fatty acid methyl esters (FAMEs), including PAME, are synthesized in various animal tissues, such as the lung (Zatz et al., 1981), pancreas (Leikola et al., 1965; Lough and Garton, 1968), retinas, and parotid (Kloog et al., 1982). However, the precursors and/or exact methyl transferases involved remain unknown. Previous studies on a rat model (Kaphalia et al., 1995) and human hepatoma HepG2 cells (Kaphalia et al., 1999) have demonstrated that endogenous FAMEs are synthesized following exposure to methanol, suggesting that carboxylesterase (EC 3.1.1.1) is a FAME methyltransferase. However, carboxylesterase is an AdoMet-independent enzyme, and its methylation usually requires external methanol. Therefore, to avoid the additional impact of methanolic solvents, we did not use methanol in our incubation experiments for PAME biosynthesis.

COMT is implicated in hypertension and cardiovascular diseases (Houston, 2007). COMT expression and activity decrease in hypertensive patients resulting in elevated circulating epinephrine and norepinephrine levels (Hirano et al., 2007) and depleted 2-methoxyestradiol (a vasodilator) levels (Hernandez et al., 2013). The decreased COMT level further increases systemic arterial pressure. Previous studies have reported that COMT expression and activity

are reduced in the liver (Tsunoda et al., 2003), brain (Masuda et al., 2006) and renal cortex (Ooshima et al., 2009) in SHRs. MB- and S-COMT expression was disproportionate in the aortic PVAT of established SHRs in parallel with PAME decrease. In addition, the plasma levels of TG and non-esterified free fatty acids, which are resources for PAME biosynthesis, were lower in 3-month-old male SHRs than in age-matched male WKY rats. (Galvez et al., 2006). Consequently, decreased COMT expression in PVAT and fat contents in adipocytes might contribute to inhibition of PAME biosynthesis, and this might be a relevant factor in hypertension pathogenesis.

PVAT dysfunction in the hypertensive state is characterized by the loss of the anti-contractile activity of PVAT (Lee et al., 2011). PVAT, which plays a paracrine role in regulating vasomotor function, releases vasodilators or vasoconstrictors (e.g., angiotensin II). Ang II exists (Galvez-Prieto et al., 2008) and increases in PVAT of established SHRs (Lu et al., 2010; Lee et al., 2011). Therefore, in the hypertensive state, Ang II synthesis increase, and PAME biosynthesis or release decreases in PVAT, leading to decreased arterial smooth muscle relaxation (Lee et al., 2011; Wang et al., 2018). Losartan is an Ang II receptor type 1 (AT-1) receptor antagonist used to treat hypertension. Previous studies have reported that losartan treatment reverses decreased PAME release from PVAT in established SHRs (Lee et al., 2011). In addition, the Ang II pathway inhibits TG lipolysis, which is also reversed by losartan treatment (Cabassi et al., 2005). Losartan can reverse low PAME biosynthesis levels

in PVAT of established SHRs, indicating the involvement of PAME in losartan-induced antihypertension effects.

There are several limitations in this study. First, the acquisition of human tissue is restricted. Therefore, we could not study PAME biosynthesis and COMT expression in human PVAT adipocytes. Second, there is no specific antibody or inhibitor that can separate the effects of MB- from S-COMT on PAME biosynthesis. Thus, we could not determine which of the two, MB-COMT or S-COMT, is a major factor in PAME biosynthesis in PVAT.

In conclusion, we, for the first time, demonstrate that PAME is synthesized through PA methylation via the AdoMet-dependent COMT catalytic pathway in adipocytes (depicted in Figure 7). In addition, the reversal of decreased PAME generation in PVAT by losartan in hypertensive rats indicates the involvement of AT-1 receptor in PAME synthesis. The role of COMT-dependent PAME biosynthesis in AT-1 receptor-mediated blood pressure regulation remains to be determined. However, due to the vasodilative effect illustrated by Lee *et al*. (Lee et al., 2011), targeting the PAME biosynthetic pathway in PVAT might help in developing therapeutic or preventive strategies against hypertension.

Acknowledgments

We thank the laboratory member of Dr. Jih-I Yeh for assistance in culturing the 3T3-L1 cell line and Dr. Jon-Son Kuo for critical reading of the manuscript.

Author contributions

Participated in research design: Mei-Fang Chen, Tony Jer-Fu Lee and Chin-Hung Liu.

Conducted experiments: Chin-Hung Liu, Tzu-Ling Tseng, Tsung-Jen Lin and Wei-Hsiang Weng.

Performed data analysis: Chin-Hung Liu, Hao-Jen Hsu and Wei-Hsiang Weng.

Wrote or contributed to the writing of the manuscript: Chin-Hung Liu, Tony Jer-Fu Lee, Mei-Fang Chen and Hao-Jen Hsu.

Statement for conflicts of interest

The authors declare no conflict of interest.

References

Bartel RL and Borchardt RT (1984) Effects of adenosine dialdehyde on S-adenosylhomocysteine hydrolase and S-adenosylmethionine-dependent transmethylations in mouse L929 cells. *Mol Pharmacol* **25**:418-424.

Borchardt RT and Huber JA (1975) Catechol O-methyltransferase. 5. Structure-activity relationships for inhibition by flavonoids. *J Med Chem* **18**:120-122.

Cabassi A, Coghi P, Govoni P, Barouhiel E, Speroni E, Cavazzini S, Cantoni AM, Scandroglio R and Fiaccadori E (2005) Sympathetic modulation by carvedilol and losartan reduces angiotensin II-mediated lipolysis in subcutaneous and visceral fat. *J Clin Endocrinol Metab* **90**:2888-2897.

Chang CC, Hsu HJ, Yen JH, Lo SY and Liou JW (2017) A Sequence in the loop domain of hepatitis C virus E2 protein identified in silico as crucial for the selective binding to human CD81. *PLoS One* **12**:e0177383.

Chang L, Villacorta L, Li R, Hamblin M, Xu W, Dou C, Zhang J, Wu J, Zeng R and Chen YE (2012) Loss of perivascular adipose tissue on peroxisome proliferator-activated receptor-gamma deletion in smooth muscle cells impairs intravascular thermoregulation and enhances atherosclerosis. *Circulation* **126**:1067-1078.

Chou CL, Pang CY, Lee TJ and Fang TC (2013) Direct renin inhibitor prevents and ameliorates insulin resistance, aortic endothelial dysfunction and vascular remodeling in

fructose-fed hypertensive rats. *Hypertens Res* **36**:123-128.

Eringa EC, Bakker W and van Hinsbergh VW (2012) Paracrine regulation of vascular tone, inflammation and insulin sensitivity by perivascular adipose tissue. *Vascul Pharmacol* **56**:204-209.

Fesus G, Dubrovska G, Gorzelniak K, Kluge R, Huang Y, Luft FC and Gollasch M (2007) Adiponectin is a novel humoral vasodilator. *Cardiovasc Res* **75**:719-727.

Galvez-Prieto B, Bolbrinker J, Stucchi P, de Las Heras AI, Merino B, Arribas S, Ruiz-Gayo M, Huber M, Wehland M, Kreutz R and Fernandez-Alfonso MS (2008) Comparative expression analysis of the renin-angiotensin system components between white and brown perivascular adipose tissue. *J Endocrinol* **197**:55-64.

Galvez B, de Castro J, Herold D, Dubrovska G, Arribas S, Gonzalez MC, Aranguez I, Luft FC, Ramos MP, Gollasch M and Fernandez Alfonso MS (2006) Perivascular adipose tissue and mesenteric vascular function in spontaneously hypertensive rats. *Arterioscler Thromb Vasc Biol* **26**:1297-1302.

Gao YJ, Lu C, Su LY, Sharma AM and Lee RM (2007) Modulation of vascular function by perivascular adipose tissue: the role of endothelium and hydrogen peroxide. *Br J Pharmacol* **151**:323-331.

Green CD and Olson LK (2011) Modulation of palmitate-induced endoplasmic reticulum stress and apoptosis in pancreatic beta-cells by stearoyl-CoA desaturase and Elovl6. *Am J*

Physiol Endocrinol Metab **300**:E640-649.

Hernandez M, Hernandez I, Rodriguez F, Pertegal M, Bonacasa B, Salom MG, Quesada T and Fenoy FJ (2013) Endothelial dysfunction in gestational hypertension induced by catechol-O-methyltransferase inhibition. *Exp Physiol* **98**:856-866.

Hirano Y, Tsunoda M, Shimosawa T, Matsui H, Fujita T and Funatsu T (2007) Suppression of catechol-O-methyltransferase activity through blunting of alpha2-adrenoceptor can explain hypertension in Dahl salt-sensitive rats. *Hypertens Res* **30**:269-278.

Hou T, Wang J, Li Y and Wang W (2011a) Assessing the performance of the MM/PBSA and MM/GBSA methods. 1. The accuracy of binding free energy calculations based on molecular dynamics simulations. *J Chem Inf Model* **51**:69-82.

Hou T, Wang J, Li Y and Wang W (2011b) Assessing the performance of the molecular mechanics/Poisson Boltzmann surface area and molecular mechanics/generalized Born surface area methods. II. The accuracy of ranking poses generated from docking. *J Comput Chem* **32**:866-877.

Hou T and Yu R (2007) Molecular dynamics and free energy studies on the wild-type and double mutant HIV-1 protease complexed with amprenavir and two amprenavir-related inhibitors: mechanism for binding and drug resistance. *J Med Chem* **50**:1177-1188.

Houston MC (2007) The role of mercury and cadmium heavy metals in vascular disease, hypertension, coronary heart disease, and myocardial infarction. *Altern Ther Health Med*

13:S128-133.

Htun NC, Miyaki K, Song Y, Ikeda S, Shimbo T and Muramatsu M (2011) Association of the catechol-O-methyl transferase gene Val158Met polymorphism with blood pressure and prevalence of hypertension: interaction with dietary energy intake. *Am J Hypertens* **24**:1022-1026.

Jiang SJ, Liou JW, Chang CC, Chung Y, Lin LF and Hsu HJ (2015) Peptides derived from CXCL8 based on in silico analysis inhibit CXCL8 interactions with its receptor CXCR1. *Sci Rep* **5**:18638.

Kanasaki K, Palmsten K, Sugimoto H, Ahmad S, Hamano Y, Xie L, Parry S, Augustin HG, Gattone VH, Folkman J, Strauss JF and Kalluri R (2008) Deficiency in catechol-O-methyltransferase and 2-methoxyoestradiol is associated with pre-eclampsia. *Nature* **453**:1117-1121.

Kaphalia BS, Carr JB and Ansari GA (1995) Increased endobiotic fatty acid methyl esters following exposure to methanol. *Fundam Appl Toxicol* **28**:264-273.

Kaphalia BS, Green SM and Ansari GA (1999) Fatty acid ethyl and methyl ester synthases, and fatty acid anilide synthase in HepG2 and AR42J cells: interrelationships and inhibition by tri-o-tolyl phosphate. *Toxicol Appl Pharmacol* **159**:134-141.

Kawai M, Namba N, Mushiake S, Etani Y, Nishimura R, Makishima M and Ozono K (2007) Growth hormone stimulates adipogenesis of 3T3-L1 cells through activation of the

Stat5A/5B-PPARgamma pathway. *J Mol Endocrinol* **38**:19-34.

Kloog Y, Zatz M, Rivnay B, Dudley PA and Markey SP (1982) Nonpolar lipid methylation-identification of nonpolar methylated products synthesized by rat basophilic leukemia cells, retina and parotid. *Biochem Pharmacol* **31**:753-759.

Kurkela M, Siiskonen A, Finel M, Tammela P, Taskinen J and Vuorela P (2004) Microplate screening assay to identify inhibitors of human catechol-O-methyltransferase. *Anal Biochem* **331**:198-200.

Lee RH, AC ES, Possoit HE, Lerner FM, Chen PY, Azizbayeva R, Citadin CT, Wu CY, Neumann JT and Lin HW (2018) Palmitic acid methyl ester is a novel neuroprotective agent against cardiac arrest. *Prostaglandins Leukot Essent Fatty Acids*.

Lee YC, Chang HH, Chiang CL, Liu CH, Yeh JI, Chen MF, Chen PY, Kuo JS and Lee TJ (2011) Role of perivascular adipose tissue-derived methyl palmitate in vascular tone regulation and pathogenesis of hypertension. *Circulation* **124**:1160-1171.

Lee YC, Chang HH, Liu CH, Chen MF, Chen PY, Kuo JS and Lee TJ (2010) Methyl palmitate: a potent vasodilator released in the retina. *Invest Ophthalmol Vis Sci* **51**:4746-4753.

Leikola E, Nieminen E and Salomaa E (1965) Occurrence of methyl esters in the pancreas. *J Lipid Res* **6**:490-493.

Lin HW, Liu CZ, Cao D, Chen PY, Chen MF, Lin SZ, Mozayan M, Chen AF, Premkumar LS, Torry DS and Lee TJ (2008) Endogenous methyl palmitate modulates nicotinic

receptor-mediated transmission in the superior cervical ganglion. *Proc Natl Acad Sci U S A* **105**:19526-19531.

Liou JW, Chang FT, Chung Y, Chen WY, Fischer WB and Hsu HJ (2014) In silico analysis reveals sequential interactions and protein conformational changes during the binding of chemokine CXCL-8 to its receptor CXCR1. *PLoS One* **9**:e94178.

Lough AK and Garton GA (1968) The lipids of human pancreas with special reference to the presence of fatty acid methyl esters. *Lipids* **3**:321-323.

Lu C, Su LY, Lee RM and Gao YJ (2010) Mechanisms for perivascular adipose tissue-mediated potentiation of vascular contraction to perivascular neuronal stimulation: the role of adipocyte-derived angiotensin II. *Eur J Pharmacol* **634**:107-112.

Ma Z, Liu H and Wu B (2014) Structure-based drug design of catechol-O-methyltransferase inhibitors for CNS disorders. *Br J Clin Pharmacol* **77**:410-420.

Mannisto PT and Kaakkola S (1999) Catechol-O-methyltransferase (COMT): biochemistry, molecular biology, pharmacology, and clinical efficacy of the new selective COMT inhibitors. *Pharmacol Rev* **51**:593-628.

Masuda M, Tsunoda M and Imai K (2006) Low catechol-O-methyltransferase activity in the brain and blood pressure regulation. *Biol Pharm Bull* **29**:202-205.

Ooshima K, Ozaki S, Tabuchi M, Higashino H, Honda E, Park AM, Arima S and Munakata H (2009) Decreased expression of catechol-O-methyltransferase in the renal cortex of

malignant spontaneously hypertensive rats. *Tohoku J Exp Med* **219**:331-336.

Peng G, Li L, Liu Y, Pu J, Zhang S, Yu J, Zhao J and Liu P (2011) Oleate blocks palmitate-induced abnormal lipid distribution, endoplasmic reticulum expansion and stress, and insulin resistance in skeletal muscle. *Endocrinology* **152**:2206-2218.

Schuttelkopf AW and van Aalten DM (2004) PRODRG: a tool for high-throughput crystallography of protein-ligand complexes. *Acta Crystallogr D Biol Crystallogr* **60**:1355-1363.

Song W, Luo Q, Zhang Y, Zhou L, Liu Y, Ma Z, Guo J, Huang Y, Cheng L, Meng Z, Li Z, Zhang B, Li S, Yee SW, Fan H, Li P, Giacomini KM and Chen L (2019) Organic cation transporter 3 (Oct3) is a distinct catecholamines clearance route in adipocytes mediating the beiging of white adipose tissue. *PLoS Biol* **17**:e2006571.

Stanley JL, Andersson IJ, Poudel R, Rueda-Clausen CF, Sibley CP, Davidge ST and Baker PN (2012) Sildenafil citrate rescues fetal growth in the catechol-O-methyl transferase knockout mouse model. *Hypertension* **59**:1021-1028.

Stewart SH, Oroszi G, Randall PK and Anton RF (2009) COMT genotype influences the effect of alcohol on blood pressure: results from the COMBINE study. *Am J Hypertens* **22**:87-91.

Szasz T, Bomfim GF and Webb RC (2013) The influence of perivascular adipose tissue on vascular homeostasis. *Vasc Health Risk Manag* **9**:105-116.

Tano JY, Schleifenbaum J and Gollasch M (2014) Perivascular adipose tissue, potassium channels, and vascular dysfunction. *Arterioscler Thromb Vasc Biol* **34**:1827-1830.

Tehlivets O (2011) Homocysteine as a risk factor for atherosclerosis: is its conversion to s-adenosyl-L-homocysteine the key to deregulated lipid metabolism? *J Lipids* **2011**:702853.

Tse EK, Salehi A, Clemenzi MN and Belsham DD (2018) Role of the saturated fatty acid palmitate in the interconnected hypothalamic control of energy homeostasis and biological rhythms. *Am J Physiol Endocrinol Metab* **315**:E133-E140.

Tseng TL, Chen MF, Liu CH, Pang CY, Hsu YH and Lee TJ (2016) Induction of endothelium-dependent constriction of mesenteric arteries in endotoxemic hypotensive shock. *Br J Pharmacol* **173**:1179-1195.

Tseng TL, Chen MF, Tsai MJ, Hsu YH, Chen CP and Lee TJ (2012) Oroxylin-A rescues LPS-induced acute lung injury via regulation of NF-kappaB signaling pathway in rodents. *PLoS One* **7**:e47403.

Tsunoda M, Tenhunen J, Tilgmann C, Arai H and Imai K (2003) Reduced membrane-bound catechol-O-methyltransferase in the liver of spontaneously hypertensive rats. *Hypertens Res* **26**:923-927.

Vieira-Coelho MA and Soares-da-Silva P (1999) Effects of tolcapone upon soluble and membrane-bound brain and liver catechol-O-methyltransferase. *Brain Res* **821**:69-78.

Wang N, Kuczmanski A, Dubrovska G and Gollasch M (2018) Palmitic Acid Methyl Ester and Its Relation to Control of Tone of Human Visceral Arteries and Rat Aortas by Perivascular Adipose Tissue. *Front Physiol* **9**:583.

Wojcicka G, Jamroz-Wisniewska A, Atanasova P, Chaldakov GN, Chylinska-Kula B and Beltowski J (2011) Differential effects of statins on endogenous H2S formation in perivascular adipose tissue. *Pharmacol Res* **63**:68-76.

Xu A, Wang Y, Lam KS and Vanhoutte PM (2010) Vascular actions of adipokines molecular mechanisms and therapeutic implications. *Adv Pharmacol* **60**:229-255.

Xu L, Li Y, Sun H, Li D and Hou T (2013) Structural basis of the interactions between CXCR4 and CXCL12/SDF-1 revealed by theoretical approaches. *Mol Biosyst* **9**:2107-2117.

Yeh JC, Borchardt RT and Vedani A (1991) A molecular model for the active site of S-adenosyl-L-homocysteine hydrolase. *J Comput Aided Mol Des* **5**:213-234.

Zatz M, Dudley PA, Kloog Y and Markey SP (1981) Nonpolar lipid methylation. Biosynthesis of fatty acid methyl esters by rat lung membranes using S-adenosylmethionine. *J Biol Chem* **256**:10028-10032.

Footnotes

This work was supported by grants from Tzu Chi Medical Foundation [TCMMP104-01-04], National Health Research Institutes [NHRI-EX104-10232SI], and the Ministry of Science and Technology [MOST105-2320-B-303-001-MY3 and MOST106-2320-B-320-011-] of Taiwan.

Deceased Author

† Professor Tony Jer-Fu Lee passed away on February 15th, 2018.

Figure Legends

Figure 1. Computational molecular modeling analysis of S-COMT with PA, DHAP and DNC. (A) Cartoon representation showing the structure of soluble (S)-COMT adopted from Protein Data Bank (code: 3A7E). The binding pockets for PA, AdoMet, and Mg^{2+} are indicated. (B) Root-mean-square deviation (RMSD) was plotted as a function of simulation times representing S-COMT–PA (blue line), S-COMT–DHAP (black line), and S-COMT–DNC (red line) interactions. (C) Hypothetic scheme showing COMT-catalyzed PAME biosynthesis. Tocalpone, AdoHcy and Adox are inhibitors for the respective enzymes as indicated. Ado, adenosine; AdoHcy, *S*-(5'-adenosyl)-*L*-homocysteine; AdoMet, *S*-5'-adenosyl-*L*-methionine; Adox, adenosine-2',3'-dialdehyde; COMT, catechol-*O*-methyltransferase; DHAP, 3,4-dihydroxyacetophenone; DNC, dinitrocatechol; Hcy, *L*-homocysteine; Met, *L*-methionine; PA, palmitic acid; PAME, palmitic acid methyl ester.

Figure 2. COMT-catalyzed PAME synthesis. (A) Generation of *O*-methylated products of DHAP (open bars) and [$^{13}C_{16}$]-PAME (solid bars) under the condition listed on the plot. The contents of the test tubes are listed on the plot. – and + represent the absence and presence of AdoMet (1 mM), respectively. DHAP or [$^{13}C_{16}$]-PA (100 μM) was separately added to the test tubes, where the COMT concentration was adjusted to 0–30 units. *P < 0.05 indicates a

significant difference from the group without COMT. (B) Effect of 3T3-L1 adipocytes differentiation on [$^{13}C_{16}$]-PAME biosynthesis. [$^{13}C_{16}$]-PAME concentrations in the media were measured after 24 or 72 h of culture with 3T3-L1 adipocytes in the fibroblast (Fib) (open bars) or adipocyte (Adi) (solid bars) stage in the presence of 100 μM or 500 μM [$^{13}C_{16}$]-PA. Represetative western blots (C) and a summarized bar graph (D) for protein expression of soluble (S)- and membrane-bound (MB)-COMT in 3T3-L1 adipocytes at the Fib and Adi stages. *$P < 0.05$ vs. COMT-omitted group in (A), and vs. the respective Fib-stage group in (B) and (D). $^{\#}P < 0.05$ vs. groups treated with 100 μM [$^{13}C_{16}$]-PA in (B). $^{\&}P < 0.05$ vs. the respective 24-h-culture group in (B). Values are presented as means ± SEM. AdoMet, *S*-5'-adenosyl-*L*-methionine; COMT, catechol-*O*-methyltransferase; DHAP, 3,4-dihydroxyacetophenone; PA, palmitic acid; PAME, palmitic acid methyl ester.

Figure 3. Suppression of PAME biosynthesis by COMT and AdoHcy hydroxylase inhibitors in 3T3-L1 adipocytes. (A) Differentiated 3T3-L1 adipocytes were incubated in a culture medium containing [$^{13}C_{16}$]-PA plus AdoHcy (A), Adox (A), or tolcapone (B) for 48 h. The levels of endogenous PAME (open bars) and [$^{13}C_{16}$]-PAME (solid bars) under the conditions indicated on the graph were measured using GC–MS. – and + represents the absence and presence of 3T3-L1 adipocytes or inhibitors, respectively. Values are means ± SEM. $^{*}P < 0.05$ vs. the control group. PA, palmitic acid; PAME, palmitic acid methyl ester;

COMT, catechol-*O*-methyltransferase; AdoHcy, *S*-(5'-adenosyl)-*L*-homocysteine; Adox, adenosine-2',3'-dialdehyde.

Figure 4. A cross-sectioned aortic ring showing the relative location of PVAT to the aortic wall. The aortic specimen was taken from a Sprague-Dawley rat and processed with hematoxylin-eosin Y staining. The layers in the aortic ring were labeled on the plot. Scale bar = 250 μm.

Figure 5. Decreased COMT expression and PAME biosynthesis in isolated aortic PVATs of SHRs. (A) Time-dependent accumulation of [$^{13}C_{16}$]-PAME in Krebs-Henseleit solution containing isolated PVAT obtained from WKY rats and SHRs for 1–90 min-incubation in the presence of 250 μM [$^{13}C_{16}$]-PA. (B) The area under each curve (AUC), which represents cumulative [$^{13}C_{16}$]-PAME generation, under the different drug pretreatment was summarized. Ages and respective marks are indicated on the plot. – and + represent the absence and presence of 1 μM losatran or tolcapone, respectively. (C and D) Membrane-bound (MB)- and soluble (S)-COMT expression in aortic PVAT of 8- or 13-week-old SHRs and WKY rats (n = 4–5). α-Tubulin levels were served as the loading control. Values are presented as means ± SEM. $^{*}P < 0.05$ indicates significant difference from the 8-week-old group without treatment. $^{\#}P < 0.05$ indicates significant difference from age-matched WKY rats. $^{\&}P < 0.05$ indicates

significant difference from the age-matched group without losartan treatment. $^{\S}P < 0.05$ indicates significant difference from the age-matched group without tolcapone treatment. COMT, catechol-*O*-methyltransferase; PAME, palmitic acid methyl ester; PVAT, perivascular adipose tissue; SHR, spontaneously hypertensive rat; WKY, Wistar Kyoto; AUC, area under the curve.

Figure 6. COMT immunoreactivity in PVAT adipocytes. (A and B) Representative images showing a aortic section immunostained with COMT and DAPI. (C) A merged image indicating the location of COMT enzyme and nuclei. The area in the red box was enlarged and presented in (D). Arrows indicate COMT-immunoreactive adipocytes, and a star indicates the presence of lipid droplet. COMT, catechol-*O*-methyltransferase; PVAT, perivascular adipose tissue; DAPI, 4',6-diamidino-2-phenylindole.

Figure 7. A schematic diagram depicting PAME biosynthesis in PVAT adipocytes. PA is produced from the lipolysis of triacylglycerol in PVAT adipocytes. PA is subsequently *O*-methylated to form PAME by MB- or S-COMT. After released from PVAT, PAME may modulate the vascular smooth muscle activity. PAME, palmitic acid methyl ester; PVAT, perivascular adipose tissue; SMC, smooth muscle cell; PA, palmitic acid.

JPET Fast Forward. Published on February 18, 2020 as DOI: 10.1124/jpet.119.263517
This article has not been copyedited and formatted. The final version may differ from this version.

Table 1. Body weight and systolic blood pressure of SHRs and WKY rats

Age (weeks)	Strain (*n*)	Body weight (g)	SBP (mmHg)
8	**WKY (15)**	243.3 ± 28.9	114.0 ± 2.6
	SHR (15)	250.0 ± 13.2	128.1 ± 10.0
13	**WKY (7)**	321.7 ± 14.4	121.5 ± 4.2
	SHR (7)	290.0 ± 10.0*	182.1 ± 13.3*

Values are presented as means ± SEM.

*$P < 0.05$ vs. age-matched WKY rats.

SBP, systolic blood pressure; SHR, spontaneously hypertensive rat; WKY, Wistar Kyoto.

JPET Fast Forward. Published on February 18, 2020 as DOI: 10.1124/jpet.119.263517
This article has not been copyedited and formatted. The final version may differ from this version.

Table 2. Free energy values of PA, DHAP and DNC

Ligands	ΔG_{bind} (Kcal/mol)	E_{MM} (Kcal/mol)		G_{solv} (Kcal/mol)	
		Coul	vdW	PolSol	NpoSol
DHAP	122.77 ± 13.23	507.82 ± 18.75	33.53 ± 5.30	–420.66 ± 21.10	2.18 ± 0.13
DNC	–61.49 ± 14.64	258.12 ± 30.42	10.78 ± 6.60	–332.25 ± 23.18	1.85 ± 0.17
PA	–40.97 ± 20.37	474.77 ± 45.32	17.94 ± 9.66	–534.93 ± 30.28	1.26 ± 0.37

Free energy values for the interactions of DHAP, DNC or PA with S-COMT were calculated by MM/PBSA.

DHAP, 3,4-dihydroxyacetophenone; DNC, dinitrocatechol; PA, palmitic acid; ΔG_{bind}, binding free energy; E_{MM}, molecular mechanics energy; Coul, Coulomb energy model; vdW, van der Waals energy model; G_{solv}, solvation free energy; PolSol, polar solvation energy model; NpoSol, norpolar solvation energy model; MM/PBSA, Molecular Mechanics Poisson–Boltzmann Surface Area.

JPET Fast Forward. Published on February 18, 2020 as DOI: 10.1124/jpet.119.263517
This article has not been copyedited and formatted. The final version may differ from this version.

Figure 1−Chin-Hung Liu *et al.*

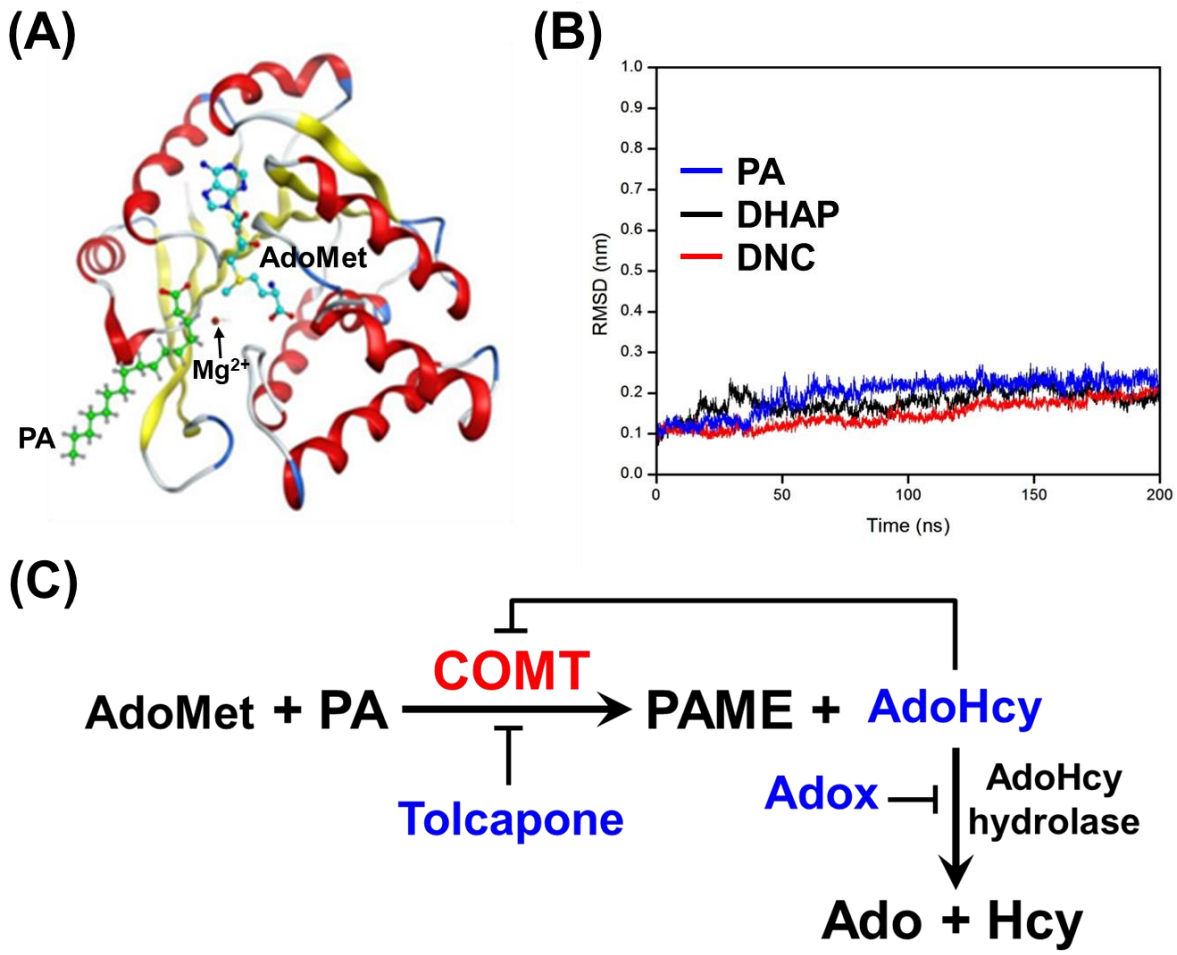

Figure 2−Chin-Hung Liu *et al.*

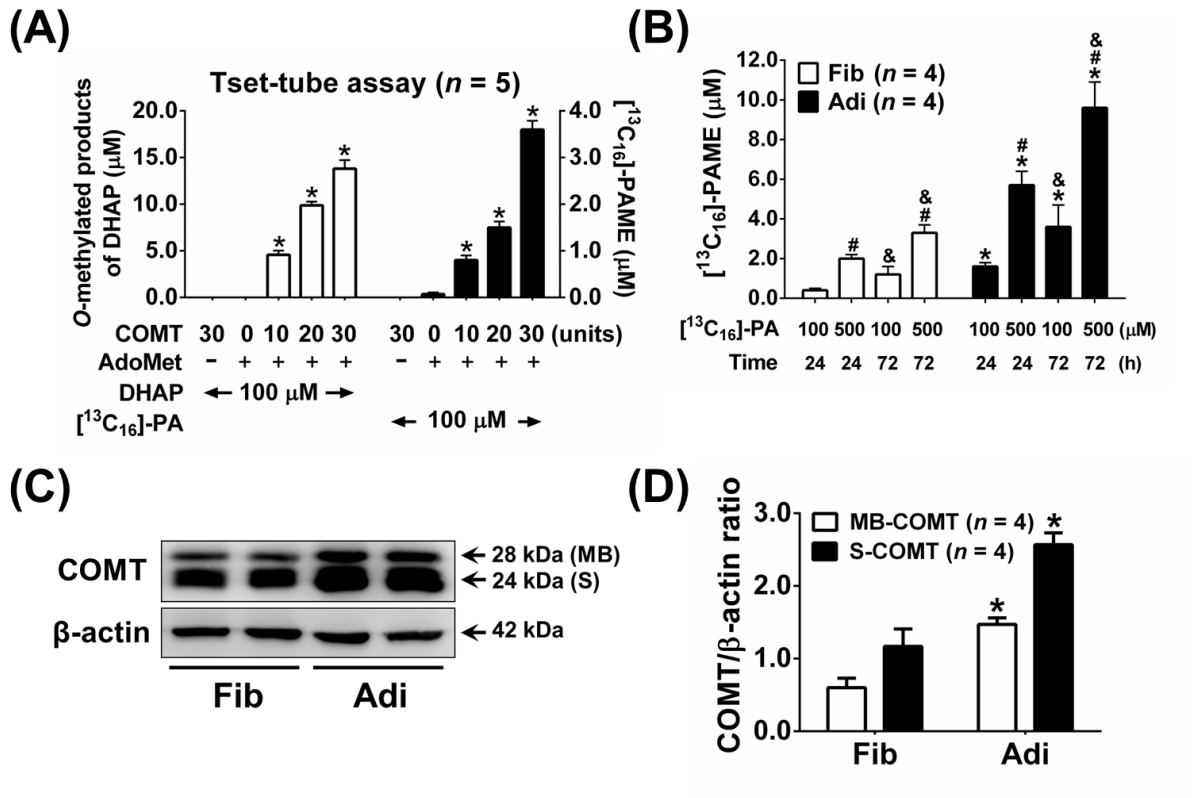

Figure 3−Chin-Hung Liu *et al.*

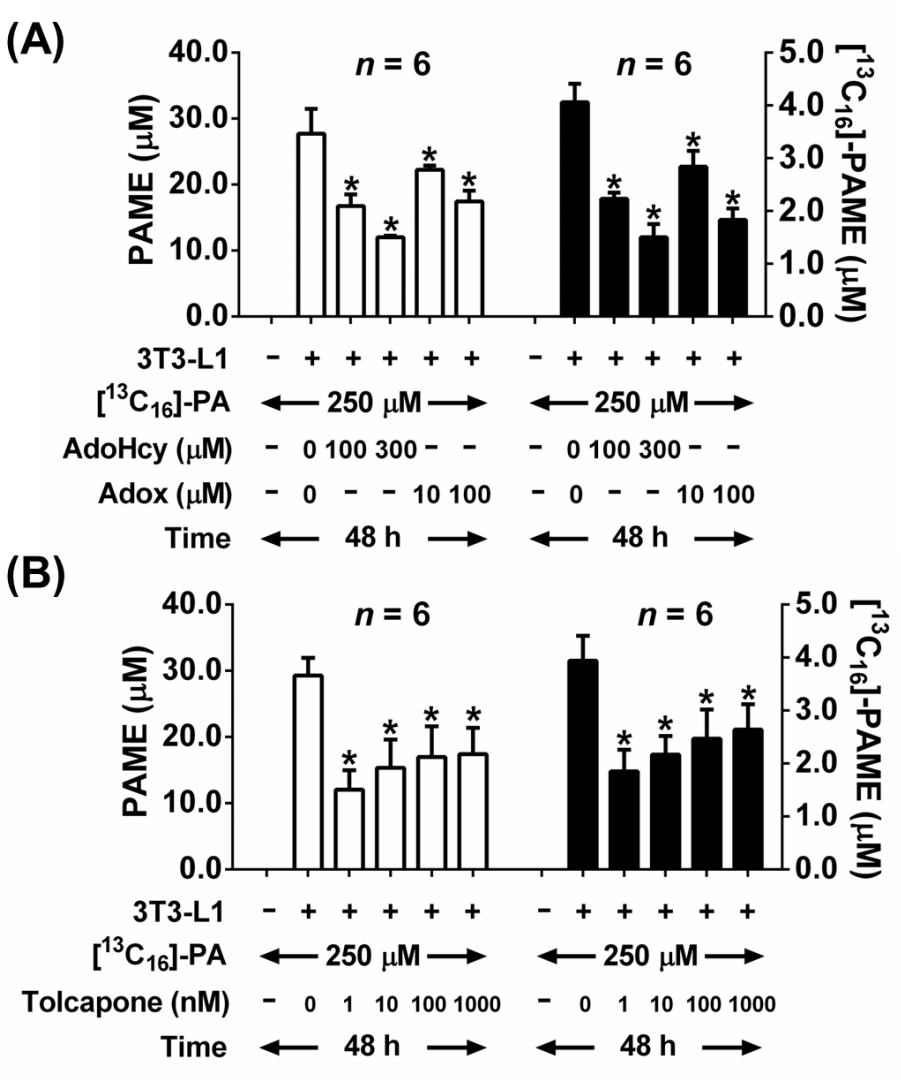

Figure 4−Chin-Hung Liu *et al.*

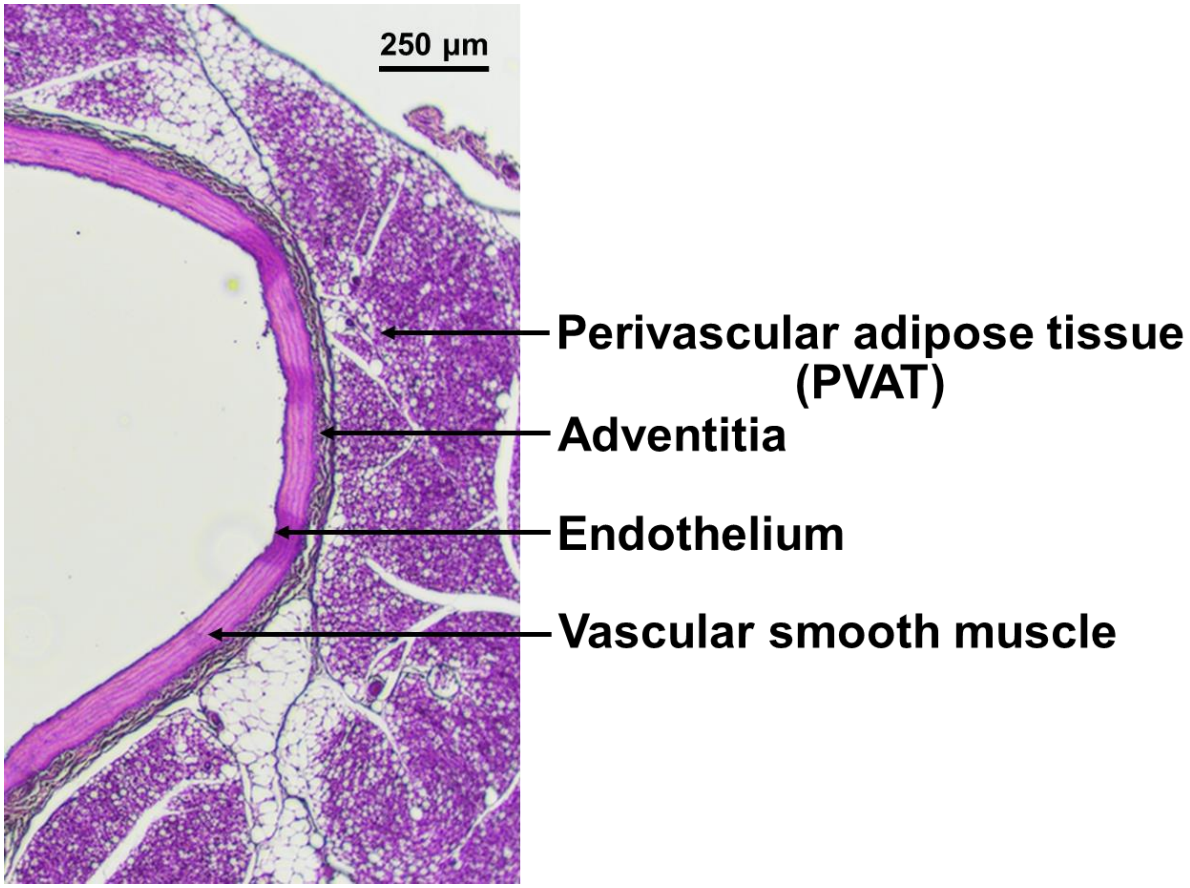

JPET Fast Forward. Published on February 18, 2020 as DOI: 10.1124/jpet.119.263517
This article has not been copyedited and formatted. The final version may differ from this version.

Figure 5−Chin-Hung Liu *et al.*

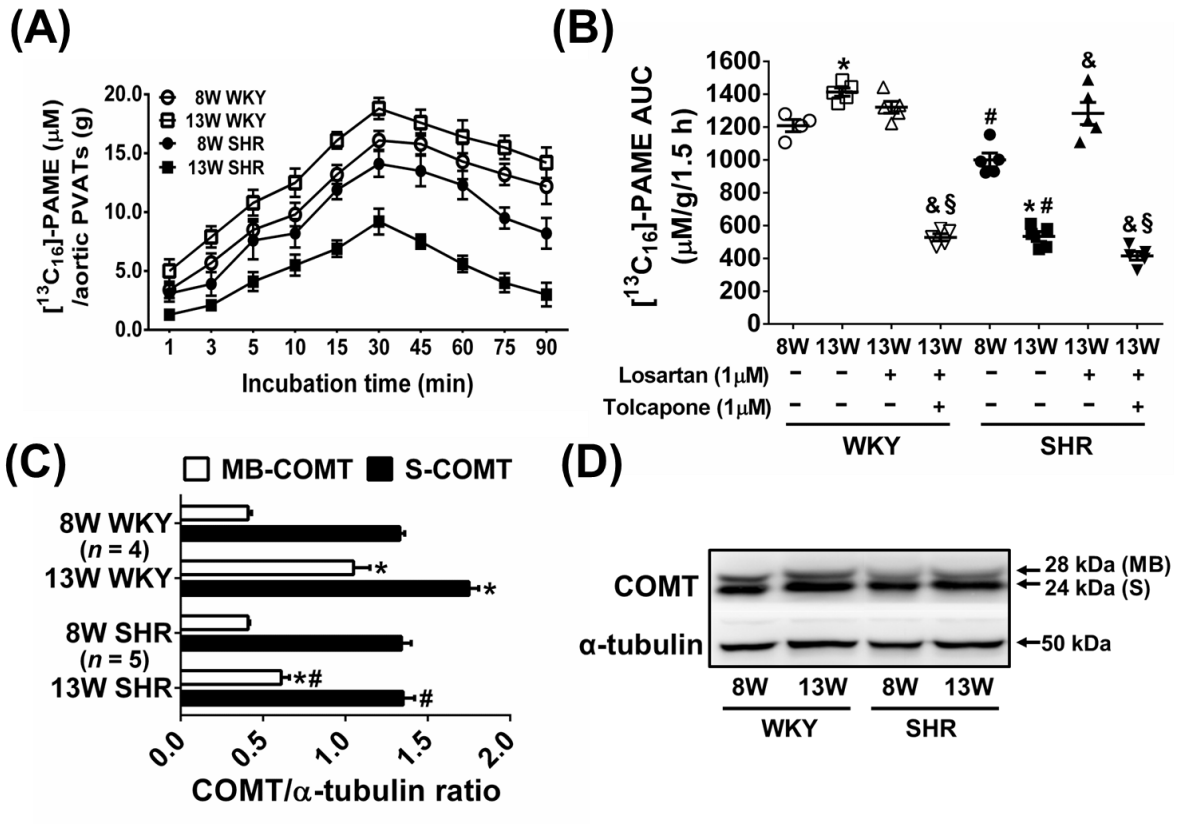

JPET Fast Forward. Published on February 18, 2020 as DOI: 10.1124/jpet.119.263517
This article has not been copyedited and formatted. The final version may differ from this version.

Figure 6−Chin-Hung Liu *et al.*

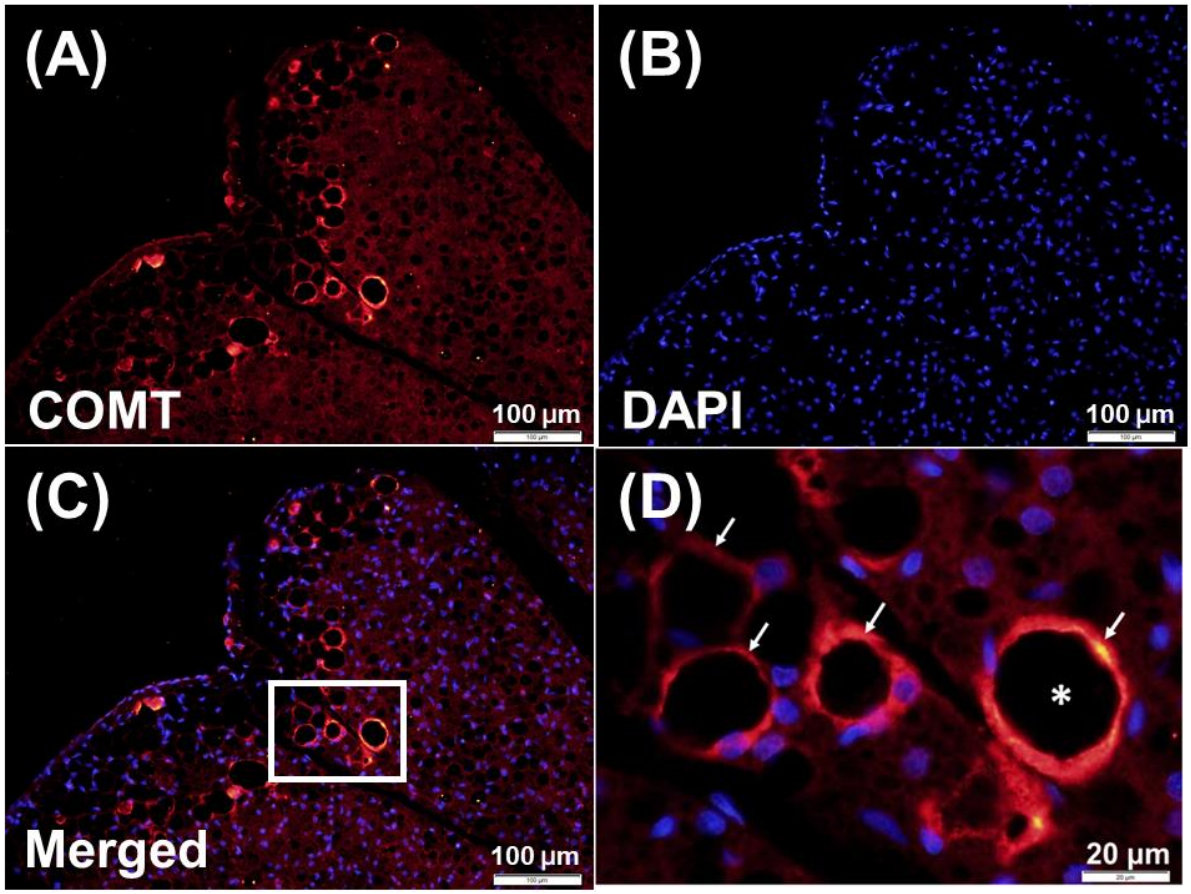

JPET Fast Forward. Published on February 18, 2020 as DOI: 10.1124/jpet.119.263517
This article has not been copyedited and formatted. The final version may differ from this version.

Figure 7−Chin-Hung Liu *et al.*

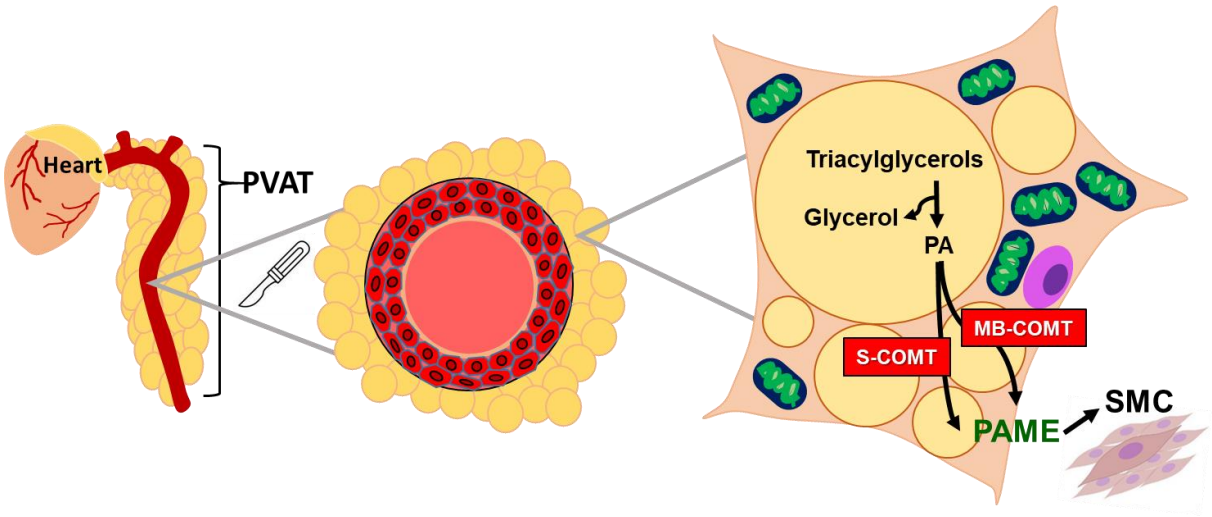

COMT-catalyzed palmitic acid methyl ester biosynthesis in perivascular adipose tissue and its potential role against hypertension

Chin-Hung Liu, Hao-Jen Hsu, Tzu-Ling Tseng, Tsung-Jen Lin, Wei-Hsiang Weng,

Mei-Fang Chen* and Tony Jer-Fu Lee*

Journal of Pharmacology and Experimental Therapeutics

Supplementary Figure 1. Ion chromatogram and mass spectra of [$^{13}C_{16}$]-PAME in GC–MS analysis. (A) In the chromatogram, peak 1, which represents PAME, and peak 2, which represents [$^{13}C_{16}$]-PAME, have identical retention time (t_R = 8.33 min). (B) The characteristic molecular ion ($[M]^+$) of PAME in the mass spectrum is 270 of *m/z* and of [$^{13}C_{16}$]-PAME (=$[M]^+$ +16) is 286 of *m/z*. Pentadecanoic acid methyl ester was used as internal standard (IS). PAME, palmitic acid methyl ester; PA, palmitic acid; GC–MS, gas chromatography–mass spectrometry.

Supplementary Figure 2. Oil Red O staining of lipid droplets in differentiated 3T3-L1 adipocytes. (A) 3T3-L1 adipocytes were stained with Oil Red O, after the differentiation of 3T3-L1 cells were induced for 6 days and subsequently maintained for additional 4 days. The red color indicates lipid droplets in the adipocytes. (B) A enlarged image from plot A.

Supplementary Figure 3. Concentration-dependent decrease in PAME biosynthesis in isolated aortic PVAT of SD rats in the presence of 300 nM or 1 μM tolcapone pre-incubation. PAME, palmitic acid methyl ester; SD, Sprague Dawley; PVAT, perivascular adipose tissue.

Supplementary Figure 4. Whole uncropped images of original western blots from Figure 2D (*n* = 4).

Supplementary Figure 5. Whole uncropped images of original western blots from Figure 5C (*n* = 4–5).

Supplementary Figure 6. Hematoxylin and eosin Y-stained cross-sections of aortic (A, C) and mesenteric PVATs (B, D). PVATs were harvested from a Sprague Dawley rat. The specimens were examined under a light microscope with magnification at 100X (A and B) and 400X (C and D). Scale bars indicate 200 μm in (A and B), and 50 μm in (C and D), respectively. PVAT, perivascular adipose tissue.

Supplementary Figure 1−Chin-Hung Liu *et al.*

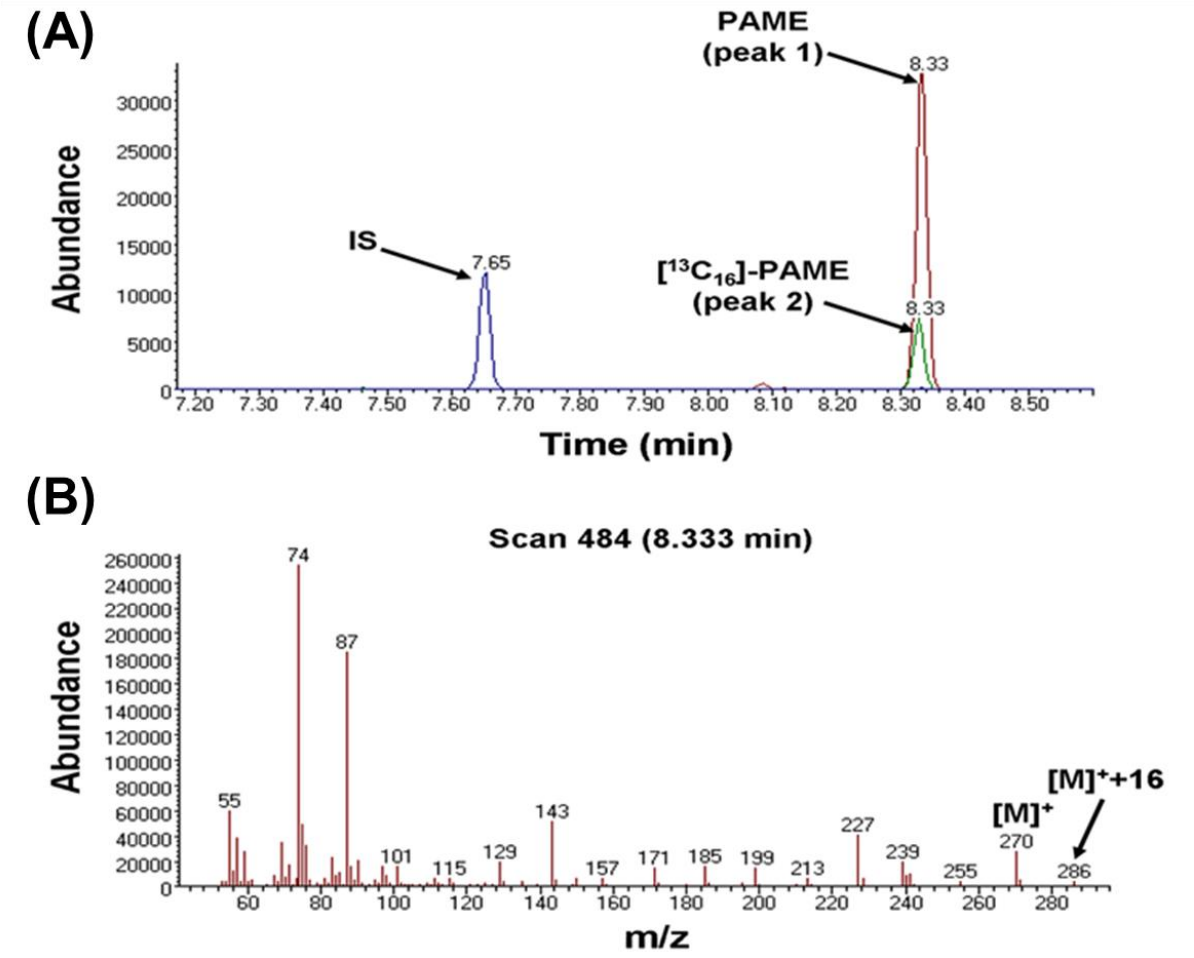

Supplementary Figure 2−Chin-Hung Liu *et al.*

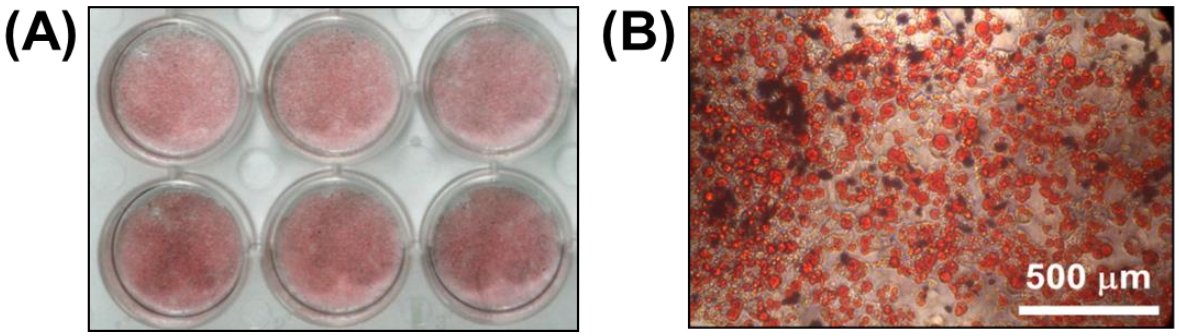

Supplementary Figure 3–Chin-Hung Liu *et al.*

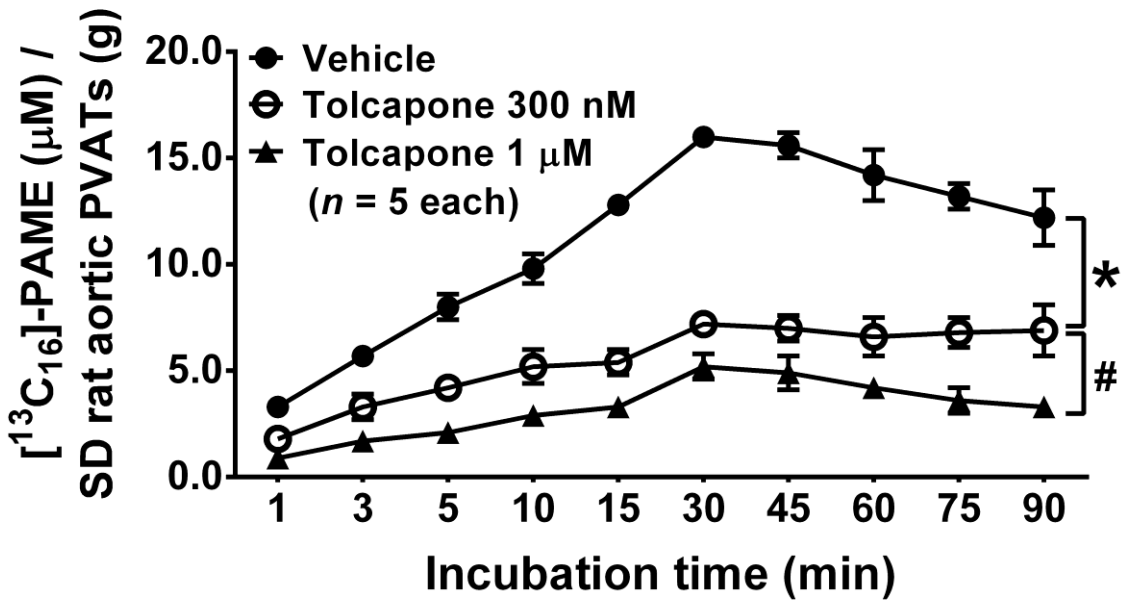

Supplementary Figure 4–Chin-Hung Liu *et al.*

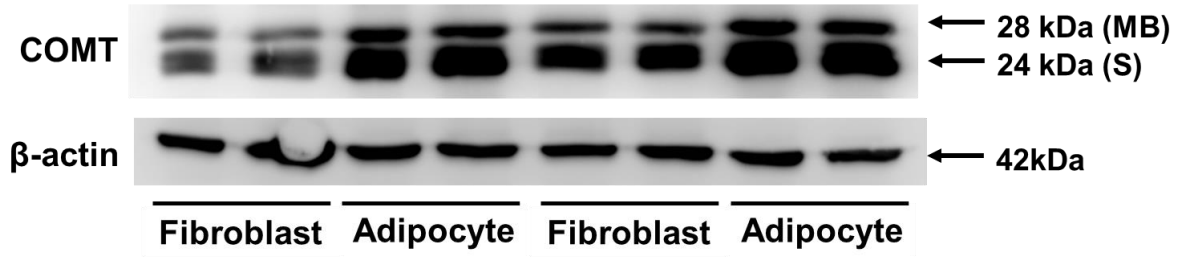

Supplementary Figure 5–Chin-Hung Liu *et al.*

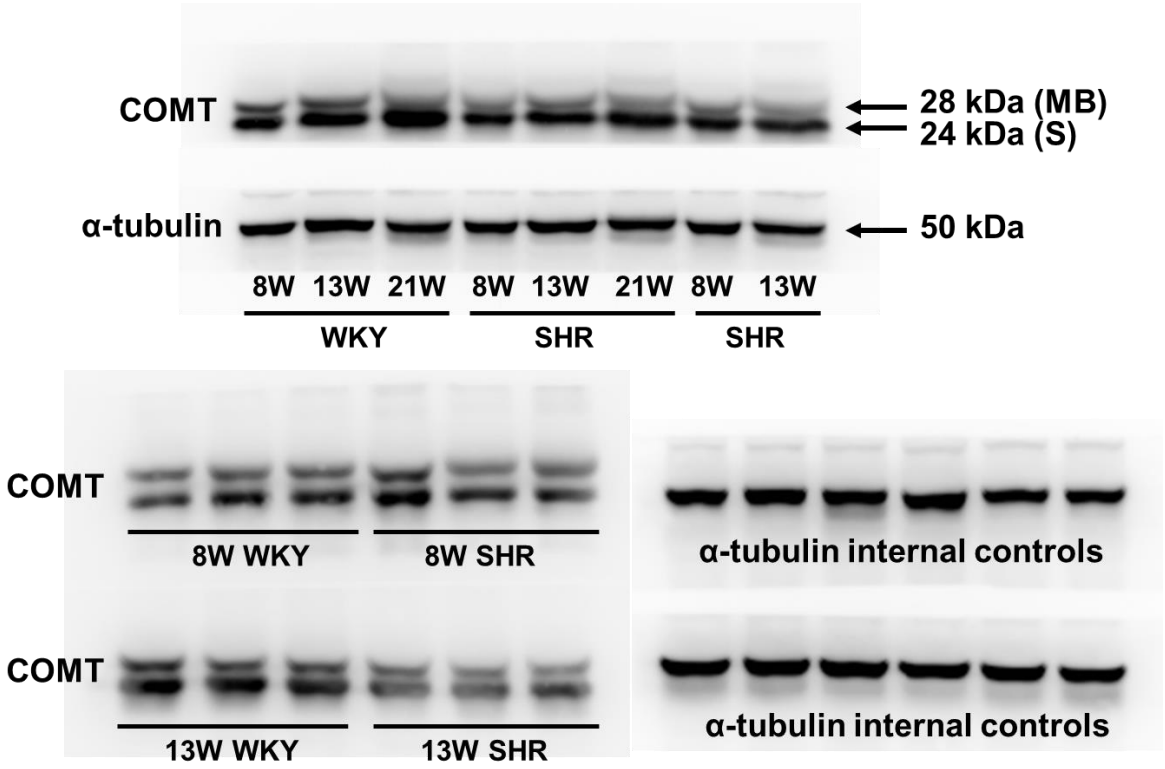

Supplementary Figure 6–Chin-Hung Liu *et al.*